Oligosaccharides Implicated in Recognition Are Predicted to Have Relatively Ordered Structures†

Andrew Almond,*,§ Bent O. Petersen,‡ and Jens Ø. Duus‡

Department of Biochemistry, University of Oxford, South Parks Road, Oxford OX1 3QU, United Kingdom, and Department of Chemistry, Carlsberg Laboratory, Gamle Carlsberg Vej 10, DK 2500 Valby, Denmark

Received August 20, 2003; Revised Manuscript Received March 3, 2004

ABSTRACT: Fucosylated O- and N-linked glycans are essential recognition molecules in plants and animals. To understand how they impart their functions, through interactions with proteins, requires a detailed analysis of structure and dynamics, but this is presently lacking. In this study, the three-dimensional structure and dynamics of three fucosylated oligosaccharides are investigated using a combination of high field (800 MHz) nuclear magnetic resonance and long (50 ns) molecular dynamics simulations in explicit water. Predictions from dynamics simulations were in agreement with nuclear Overhauser cross-peak intensities. Similarly, a theory of weak alignment in neutral media resulted in reasonable predictions of residual dipolar couplings for the trisaccharide fucosyllactose. However, for larger penta- and hexasaccharides (LNF-1 and LND-1), the anisotropic component of the alignment was underestimated, attributed to shape irregularities of the fucosyl branches on an otherwise linear core, being more pronounced in a singly branched than a doubly branched oligosaccharide. Simulations, confirmed by experiment, predicted fucosylated molecules that are restricted to librations about a single average conformation. This restriction is partly due to microscopic water interactions, which act to stabilize intramolecular hydrogen bonds and maintain tight and ordered conformations; a view not forthcoming from simpler, nonaqueous simulations. Such a conclusion is crucial for understanding how these molecules interact with proteins and impart their recognition properties.

Recent advances in X-ray crystallography and nuclear magnetic resonance (NMR)[1] have vastly improved knowledge of static, time-averaged molecular structure (*1*). Although profound, these models of three-dimensional structure provide little insight into the mechanisms and energies involved in macromolecular interactions, which result from dynamic interplay (*2*, *3*). Unfortunately, the study of dynamics in macromolecules is often hindered by the large number of dynamic degrees of freedom which outweigh the experimental observables. Such difficulties have driven structural biologists to concentrate their efforts on the more tangible and defined goal of interpreting molecular structure in terms of well-defined single conformations.

The interpretation of complex carbohydrates in terms of rigid, well-defined conformations is not a good approximation (*4*). This, compounded with the fact that molecular motions exist on the nanosecond time scale in carbohydrates, a time scale that virtually escapes direct experimental probing, makes the computer an extremely useful tool for investigating their three-dimensional structure and dynamics. However, the strong interaction of carbohydrates with water necessitates the inclusion of solvent in any simulation of microscopic dynamics. At present, the most realistic models of water are those that include individual molecules, but they are also the most computationally demanding (*5*). This has previously limited the extent of accurate simulations of carbohydrate molecules, creating an undesirable gap between experimental data and what simulations could predict. Technological developments allow accurate simulations to be performed which are extensive enough to start bridging this gap. Such simulations significantly improve the interpretation of experimental data in terms of dynamic structure. In particular, residual dipolar couplings, measured by NMR in the partially aligned solution phase, are suitable for incorporation into a combined theoretical and experimental approach to studying dynamics.

Fucosylated oligosaccharides represent an ideal target for such methodology, since the terminal regions of these molecules are involved in important biological recognition phenomena. They form the basis of fundamental blood group antigens, and are implicated in a wide variety of biological phenomena, including fertilization, development, cell adhesion, apoptosis, and cancer progression (*6*). For this reason, fucosylated oligosacchardes have been the subject of a wide variety of conformational investigations. These include NMR studies in the free solution (*7*, *8*) and partially aligned state (*9*, *10*), simple molecular modeling studies (*11*−*14*), and X-ray diffraction in complex with proteins (*15*).

† This research was carried out with the aid of a Wellcome Trust (U. K.) Prize Travelling Research Fellowship (to A.A.), Grant Reference No. 058154.

* To whom correspondence should be addressed. E-mail: Andrew.Almond@bioch.ox.ac.uk.

§ University of Oxford.

‡ Carlsberg Laboratory.

[1] Abbreviations: NMR, nuclear magnetic resonance; NOE, nuclear Overhauser enhancement; RDC, residual dipolar coupling; NOESY, nuclear Overhauser enhancement spectroscopy; gHSQC, gradient heteronuclear single-quantum spectroscopy; COSY, correlated spectroscopy; TOCSY, total correlated spectroscopy; Glc, D-glucose; Gal, D-galactose; GlcNAc, *N*-acetyl D-glucosamine; Fuc, L-fucose.

10.1021/bi0354886 CCC: $27.50
Published on Web 04/24/2004

Molecular dynamics simulations, with explicit solvent, have previously been used to aid the interpretation of residual dipolar couplings measured in oligosaccharides (*16*, *17*). Since then, a simple protocol has been developed to calculate alignment tensors from structure, suitable for predicting residual dipolar couplings from dynamic simulations (*18*). In this study, these techniques are utilized and extended to investigate the dynamics of lactose derivatives containing both α(1 → 2) and α(1 → 4) linked fucose. In contrast to previous studies of similar molecules (*7*−*15*), extensive molecular dynamics simulations in aqueous solution are utilized to aid the interpretation of both residual dipolar coupling and relaxation data collected from NMR experiments.

MATERIALS AND METHODS

Sample Preparation. The oligosaccharides (natural abundance nuclear isotopes) used in these studies were purchased pure from Glycorex AB (Sölvegatan 41, SE-223 70 Lund, Sweden) and used without further purification. Each had a free reducing terminus and hence was a mixture of α- and β-anomers in aqueous solution. In each case, two NMR samples of volume 600 μL (a total of six) were prepared at a concentration of 10 mg/mL oligosaccharide in D_2O, with 10 mM sodium phosphate buffer (pD 7.6 uncorrected) and 2 mM magnesium chloride. To one of the samples of each oligosaccharide Pf1 phages were added. In the case of fucosyllactose, the concentration of phage was adjusted to give a ^2H quadrupolar splitting of D_2O of 18 Hz at 300 K, providing residual dipolar couplings in the required range. For LNF-1 and LND-1, the concentration of phage was reduced to give a ^2H splitting of 8 Hz, as it was observed that these molecules aligned more readily. Phages were purchased from ASLA Biotech Ltd. (Bauskas 121, Riga, LV-1004, Latvia).

Nuclear Magnetic Resonance. All NMR spectra were recorded on a Varian Unity Inova 800 MHz spectrometer. Homonuclear ^1H COSY and TOCSY were recorded for each sample in the absence of phage, to yield the ^1H assignments. A spectral width of 6 kHz was used in both dimensions, with 4096 complex points in the direct dimension and 512 complex points in the indirect dimension. Water suppression was achieved using light presaturation during the recycle delay. The corresponding carbon assignments were obtained from standard ^1H-^{13}C gHSQC experiments, using sweep widths of 3 and 12 kHz in proton and carbon dimensions respectively, and acquisition of 4096 (direct proton) and 512 (indirect carbon) complex points. This increased the spectral resolution in the direct dimension by folding some of the outlying peaks. For measurements of coupling constants, the corresponding gHSQC experiments were performed with the same number of points, but the carbon sweep width was reduced to 8.5 kHz, allowing peaks to fold into empty regions in the indirect dimension. All HSQC spectra were zero-filled to twice the number of points prior to the Fourier transform. The NOESY spectra were recorded in the absence of phage using a configuration similar to the COSY and TOCSY experiments, with a mixing time of 800 ms in all cases. All spectra were zero-filled to double the number of points in both dimensions prior to processing.

For measurement of one-bond couplings, the standard ^1H-^{13}C gHSQC sequence was modified, removing decoupling during the observation period. This allowed the one-bond ^1H-^{13}C couplings (c. 100 Hz) to be observed in the direct dimension. Good spectral dispersion rendered it unnecessary to use more complicated pulse sequences, such as spin-state-selective coherence transfer (*19*), to measure virtually all of the ^1H-^{13}C one-bond couplings. Spectra were recorded with and without the presence of phage, and residual dipolar couplings were inferred from the difference in measured one-bond couplings between the two spectra. However, it was found that the line-shapes of the α and β spin-doublet components of a single resonance often differed (see Figure 1), which was attributed to strong coupling effects (*20*). Therefore, to minimize errors, the β resonances were overlaid in the aligned and nonaligned cases (which are similar except for line broadening), and then the distance between the two other α resonances were measured. This is equal to the residual dipolar coupling, but never requires the distance between an α and β resonance to be measured.

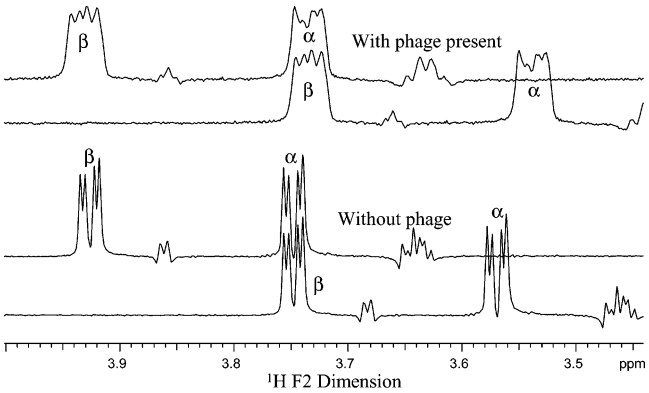

FIGURE 1: Examples of 1D spectra extracted from 2D ^1H-^{13}C HSQC spectra used to measure one-bond residual dipolar couplings. All spectra show slices through fucosyllactose β-Gal C3; the top traces show spectra in aligned phages, and the bottom traces spectra in free solution. In each case, two similar 1Ds have been overlaid, and one has been shifted so that the α resonance coincides with the β of a CH spin doublet; the necessary shift is the effective coupling between the C and H nuclei.

Molecular Dynamics Simulations. Simulations used an all-atom approach in which the atoms were represented as van der Waals spheres with a partial charge. Bonds were represented using the approach of molecular mechanics, and a force-field suitably modified for carbohydrates (*21*). In this representation, torsional terms are calculated from ab initio molecular orbital calculations, to which force-field parameters are empirically fitted. The force-field can then correctly reproduce torsional potentials for α- and β-glycosidic linkages predicted by quantum calculations, using suitable partial atomic charges. In this case, partial charges were precalculated by least-squares fitting to quantum mechanical electrostatic potentials, calculated with the HF/6-31G* basis set.

Molecular dynamics simulations were performed using the CHARMm program (*22*). In all cases, explicit water was modeled using 1500 TIP3P water molecules (*23*) equilibrated at 300 K. To maintain the correct density and simulate long-range electrostatics, periodic boundary conditions were applied with rhombic dodecahedral symmetry, of unit cell length 3.996 nm. Electrostatics were treated using a group based cutoff switched between 0.8 and 1.2 nm. Following equilibration (for 200 ps), during which the system was strongly coupled to a heat bath, each simulation was

continued for 50 ns at constant temperature (300 K) and volume to construct a canonical (NVT) ensemble. Molecular dynamics integration was carried out using the leapfrog formulation (*24*) of the Verlet algorithm (*25*), and hydrogen covalent bond lengths were kept constant using the SHAKE procedure (*26*). An integration step size of 2 fs was used, with no explicit hydrogen-bonding function. Full coordinate sets were stored at 200 fs intervals for later analysis. Single simulations of length 50 ns were performed for fucosyllactose and LND-1. For LNF-1, two simulations of length 50 ns were performed in which the α(1 → 2) linkage was started in different conformations, $\psi = 0°$ and $\psi = 180°$ (see below for angular definitions). All other linkages were started in the region of $(\phi, \psi) \approx (50°, 30°)$. The reducing terminus of each oligosaccharide was fixed covalently into the β-configuration.

Analysis of Molecular Dynamics Simulations: Conformation and Hydrogen Bonds. Glycosidic linkage conformation was represented by dihedral angles ϕ (H1−C1−O×−C×) and ψ (C1−O×−C×−H×) defined by the hydrogen atoms at the linkages. Intramolecular hydrogen-bond interactions were assigned when the distance D (hydrogen donor) to A (hydrogen acceptor) was less than 3.5 Å, and the angle D−A···A less than 60°. This (arbitrary) definition of a hydrogen bond has been used in the analysis of other carbohydrate simulations (*27*). Following extraction, they were classified depending on their overall persistence during the simulation. Only the most persistent were kept for later analysis.

Analysis of Molecular Dynamics Simulations: Residual Dipolar Couplings. Calculation of residual dipolar couplings requires knowledge of the alignment tensor. Initially this was predicted from a theory of alignment by steric hindrance (*18*). This relies on calculation of the radius of gyration tensor, performed for each frame in the simulation. The tensor was diagonalized using standard techniques, and the diagonal components used to calculate the alignment tensor (*18*). For each frame, the molecule was transformed into the principal frame of the radius of gyration tensor and direction vectors were extracted corresponding to the experimentally measured scalar couplings. These were multiplied by the alignment tensor prediction to yield residual dipolar coupling predictions. Averaging over the whole simulations resulted in predictions which can be compared against experimental measurements.

In the second method, each frame was orientated in the principal frame of the radius of gyration tensor (allowing for comparison between frames) and each of the direction vectors corresponding to the experimentally measured scalar couplings extracted. The alignment tensor was calculated using these vectors and the experimentally measured data, by singular value decomposition (*28*). This tensor was then multiplied by the extracted direction vectors to back-calculate the residual dipolar coupling predictions. Averaging over the whole simulations resulted in predictions that can be compared against experimental measurements.

Analysis of Molecular Dynamics Simulations: NOESY Intensities. For each frame in the simulation the coordinates were extracted and the matrix of r_{ij}^{-6} calculated for all nonexchangeable protons. Using standard equations for calculating the spectral density function for dipolar interactions (Lipari and Szabo model free approach (*29*)) the relaxation matrix was calculated and solved by matrix diagonalization (*16*). This method explicitly takes into account spin-diffusion, which may be present at NOESY mixing times of 800 ms. NOESY predictions were made for each frame and averaged over the whole simulation to obtain data comparable with experiment. Order parameters (S^2) were set to 1.0 and τ_c was estimated by fitting NOESY intensity predictions to experimental data for protons in fixed relative geometry, i.e., those within the same sugar residue.

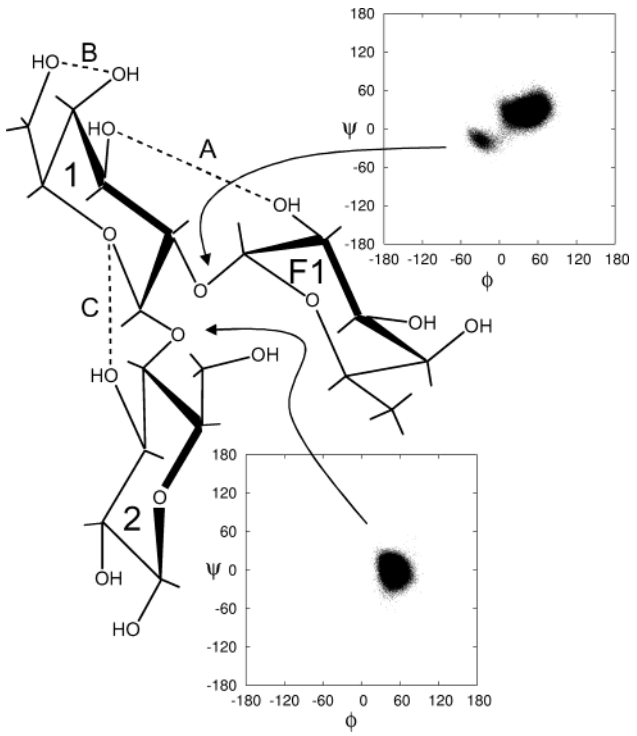

FIGURE 2: The chemical structure of the trisaccharide fucosyllactose, the predicted distribution of angles at the glycosidic linkages (see Materials and Methods for definitions) from a 50 ns molecular dynamics simulation in aqueous solution, and the predicted intramolecular hydrogen bonds.

RESULTS

Experiments and Predictions. Three fucosylated oligosaccharides were prepared as NMR samples in the free and aligned state: Fuc α(1 → 2) Gal β(1 → 4) Glc, subsequently referred to as fucosyllactose, Fuc α(1 → 2) Gal β(1 → 3) GlcNAc β(1 → 3) Gal β(1 → 4) Glc, referred to as LNF-1, and Fuc α(1 → 2) Gal β(1 → 3) [Fuc α(1 → 4)] GlcNAc β(1 → 3) Gal β(1 → 4) Glc, referred to as LND-1. Detailed NMR preparation methods are described in the Materials and Methods, and chemical structures of the oligosaccharides are shown schematically in Figures 2−4. In these figures, and in the subsequent text, the numbering of sugars runs sequentially from the nonreducing termini of the oligosaccharides, with the exception of α(1 → 2) and α(1 → 4) linked fucose, which are labeled F1 and F2, respectively. Chemical shift assignments for both proton and carbon nuclei were made with the aid of COSY, TOCSY, NOESY, and gHSQC experiments at 800 MHz proton frequency. The experimental details are provided in Materials and Methods, and the assignments are listed as Supporting Information. The assignments are in agreement with those published previously, but at lower fields (*8*, *10*, *30*). Although the hydroxymethyl groups of the hexopyranoses could be assigned, these

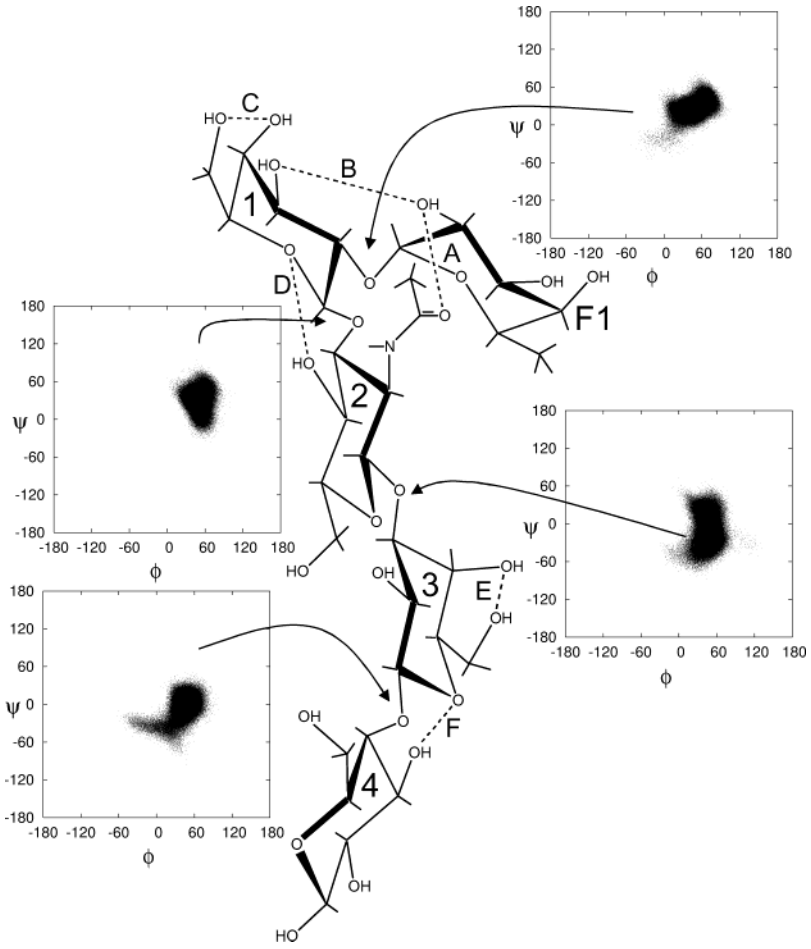

FIGURE 3: The chemical structure of the pentasaccharide LNF-1, the predicted distribution of angles at the glycosidic linkages from a 50 ns molecular dynamics simulation in aqueous solution, and the predicted intramolecular hydrogen bonds.

values are not reported, as they are not utilized further. Residual dipolar couplings were calculated from gHSQC experiments at 800 MHz, without acquisition decoupling, recorded in both the free and aligned states (as described in Materials and Methods). Figure 1 shows examples of 1D slices overlaid in the free and aligned state. The calculated one-bond residual dipolar couplings are listed in the Supporting Information; the presence of a dash indicates that overlap rendered the measurement inaccurate.

Molecular dynamics simulations, each of length 50 ns, were performed for each of the oligosaccharides detailed in Figures 2−4, as described in Materials and Methods. Oligosaccharides had their reducing termini fixed in the β-anomeric configuration prior to simulation, which corresponds to the most populated state in aqueous solution. Although NMR samples consisted of a mixture of α- and β-anomers, and both could be assigned, interpretation is restricted to the β-anomer. Glycosidic torsion angles (termed ϕ and ψ) were recorded for each of the linkages at a frequency of 0.2 ps. These data were used to construct two-dimensional plots of ϕ against ψ for every linkage. Results for fucosyllactose, LNF-1, and LND-1 have been included in Figures 2, 3, and 4, respectively.

Comparison with NOESY Measurements. Predictions of NOESY cross-peak intensities were made using standard relaxation equations and the Lipari-Szabo assumption (*29*) for calculating spectral density functions. Experimental NOESY measurements were performed using two-dimensional techniques at 800 MHz (see Materials and Methods). The theoretical predictions made for each oligosaccharide, and comparison with experimental data is shown in Tables 1−3. Fitting of the theoretical predictions to the experimental data resulted in the estimation of an empirical parameter τ_c, the overall rotational tumbling time, which is theorized to be related to molecular size, assuming the molecules tumble isotropically. It is has been proposed that τ_c is approximately proportional to the solvent accessible surface area to some power (*31*), which is, for example, 3/2 for roughly spherical objects. The solvent accessible surface areas of fucosyllactose, LNF-1 and LND-1 were estimated at 614, 1024, and 1069 Å^2, respectively. This is in qualitative agreement with the fits, which estimated τ_c to be 0.31, 0.41, and 0.50 ns, respectively.

In fucosyllactose, the important NOESY cross-peak between Fuc H1 and Gal H2 was observed experimentally, and is also predicted by the simulation, supporting the theoretical conformation at the α(1 → 2) linkage, see Table 1. Similarly the simulation predicts a NOESY cross-peak between Gal H1 and Glc H4 at the β(1 → 4) linkage. However, this could not be observed by 2D NOESY spectroscopy due to overlap. Otherwise, all measured NOEs were predicted by the simulation. Slight systematic discrencies between the experimental data and theoretical are expected due to breakdown of the isotropic tumbling model and the fact that internal motion cannot be completely deconvoluted from tumbling in flexible molecules (*16*).

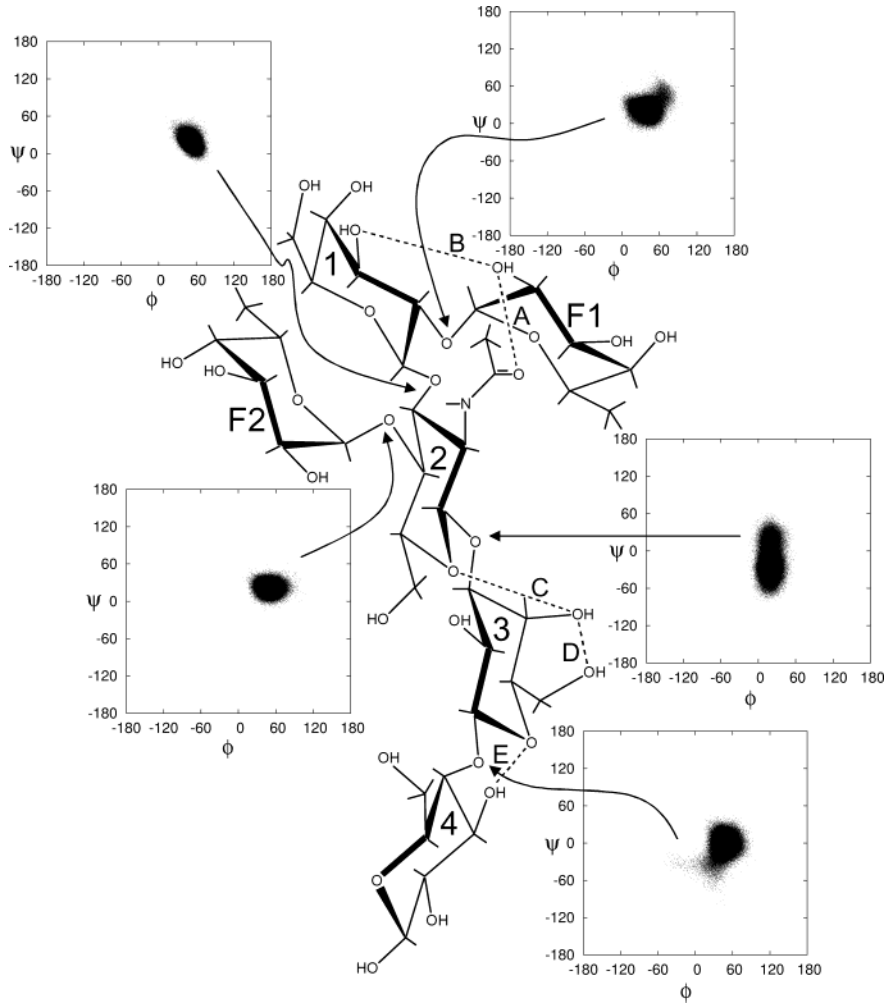

FIGURE 4: The chemical structure of the hexasaccharide LND-1, the predicted distribution of angles at the glycosidic linkages from a 50 ns molecular dynamics simulation in aqueous solution, and the predicted intramolecular hydrogen bonds.

Table 1: NOESY Measurements and Predictions for Fucosyllactose Using a Mixing Time of 800 ms[a]

residue and atom		residue and atom[b]		NOE experimental	NOE predicted[d]
1	H4	1	H5	8.0 ± 0.8	3.7
3	H5	3	H1 (β)	2.4 ± 0.2	3.1
3	H3	3	H1 (β)	1.9 ± 0.2	1.9
2	H2	1	H1	4.4 ± 0.4	3.1
3	H5 (β)	1	H5	1.7[c] ± 0.2	2.1

[a] Residues F1, 1 and 2 are Fuc, Gal, and Glc, respectively (χ^2 = 55.7, 5 points). A NOESY cross-peak was predicted between 2H1 and 3H4, but could not be observed in the 2D spectra due to overlap. [b] NOESY cross-peaks were normalized against the diagonal peak corresponding to the atom described in the second set of columns. [c] Measured intensity multiplied by 1.5 to take account of the anomeric α/β population ratio. [d] Theoretical calculation, assuming no internal motion and isotropic tumbling, τ_c = 0.31 ns, normalizing against the diagonal peak intensity.

In the case of LNF-1, all of the major linkage conformation-defining NOESY cross-peaks were observed experimentally: $\alpha(1 \rightarrow 2)$, Fuc H1 to Gal H2, $\beta(1 \rightarrow 3)$, Gal H1 to GlcNAc H3, $\beta(1 \rightarrow 3)$, GlcNAc H1 to H3, and $\beta(1 \rightarrow 4)$, Gal H1 to Glc H4. Two simulations of LNF-1 were performed, one with the fucose $\alpha(1 \rightarrow 2)$ linkage starting in a conformation with $\psi = 0°$ and the other with $\psi = 180°$. During the simulations, no exchange between the two conformers was observed. Table 2 shows the NOESY predictions for simulations in the two different conformers. Using the calculated χ^2 values, it is apparent that the conformer with $\psi = 0°$ (χ^2 = 1316.4, 24 points) is in better agreement with the experimental data than the conformer with $\psi = 180°$ (χ^2 = 6231.5, 24 points). In particular, NOEs between the core of the sugar and F1 (boldfaced in Table 2) have a noticeably worse correlation to the experimental data for $\psi = 180°$ (χ^2 = 6089.2, 5 points) than for $\psi = 0°$ (χ^2 = 1102.1, 5 points). Linear combinations of the two failed to improve this correlation, and therefore based on the NOESY data it is the $\psi = 0°$ conformer that predominates; the $\psi = 180°$ conformer is therefore ignored from hereon. For the LND-1 oligosaccharide all interglycosidic NOESY cross-peaks were observed and measured. These are $\alpha(1 \rightarrow 2)$, Fuc H1 to Gal H2, $\alpha(1 \rightarrow 4)$, Fuc H1 to GlcNAc H4, $\beta(1 \rightarrow 3)$, Gal H1 to GlcNAc H4, $\beta(1 \rightarrow 3)$, GlcNAc H1 to Gal H3, and $\beta(1 \rightarrow 4)$, Gal H1 to Glc H4. Again they were predicted to be strong cross-peaks by the simulations, as shown in Table 3. It is therefore evident that the present simulations are consistent with experimental NOESY data. However, NOESY alone can lead to ambiguous predictions of molecular conformations for carbohydrates. Thus, the simulations were tested against residual dipolar coupling data.

Steric Alignment. Using methodology described previously (*16*−*18*), it is possible to use the simulations as a basis for direct predictions of residual dipolar couplings. Techniques

Table 2: NOESY Measurements and Predictions for LNF-1, Using a Mixing Time of 800 ms[a]

residue & atom		residue & atom[b]		NOE experimental	NOE theoretical[c]	
					$\psi = 0°$	$\psi = 180°$
F1	H2	F1	H1	5.5 ± 0.6	6.9	8.7
F1	H5	F1	H1	0.6 ± 0.1	0.4	0.6
F1	H3	F1	H5	4.9 ± 0.5	6.5	6.1
F1	H4	F1	H5	5.8 ± 0.6	7.5	6.9
1	H5	1	H1	6.2 ± 0.6	6.8	7.9
1	H2	1	H1	2.5 ± 0.3	1.8	2.4
1	H3	1	H1	5.7 ± 0.6	5.0	4.9
1	H4	1	H5	5.8 ± 0.6	7.2	6.6
2	H2	2	H1	2.2 ± 0.2	1.8	1.9
2	H3	2	H1	7.0 ± 0.7	2.1	3.5
2	H5	2	H1	7.7 ± 0.8	9.9	9.0
4	H3	4	H1	3.0 ± 0.3	4.0	4.0
4	H5	4	H1	7.8 ± 0.8	6.4	7.0
1	**H2**	**F1**	**H1**	**6.8 ± 0.7**	**5.8**	**0.9**
1	**H3**	**F1**	**H1**	**0.5 ± 0.1**	**0.7**	**4.3**
1	**H2**	**F1**	**H5**	**1.3 ± 0.1**	**2.4**	**0.5**
2	**H2**	**F1**	**H5**	**6.8 ± 0.7**	**4.7**	**0.0**
2	**H4**	**F1**	**H5**	**0.6 ± 0.1**	**2.5**	**0.0**
2	H3	1	H1	5.7 ± 0.6	5.6	4.3
3	H1	2	H1	0.4 ± 0.1	0.3	0.3
3	H3	2	H1	11.5 ± 1.2	9.8	9.5
3	H4	2	H1	0.8 ± 0.1	1.1	1.1
3	H3	2	H5	0.5 ± 0.1	0.9	0.7
4	H4	3	H1	11.0 ± 1.1	11.3	9.6

[a] F1 is an α(1 → 2) linked fucose. Residues 1, 2, 3, and 4 are Gal β(1 → 3), GlcNAc, Gal β(1 → 4) and Glc, respectively. The NOESY cross-peak intensities are calculated for two conformations of the α(1 → 2) linkage, one with $\psi = 0°$ ($\chi^2 = 1316.4$, 24 points) and one with $\psi = 180°$ ($\chi^2 = 6231.5$, 24 points). The boldfaced area highlights NOEs that change dramatically when ψ is varied. [b] NOESY cross-peaks were normalized against the diagonal peak corresponding to the atom described in the second set of columns. [c] Theoretical calculation, assuming no internal motion and isotropic tumbling, $\tau_c = 0.41$ ns.

Table 3: NOESY Measurements and Predictions for LND-1, Using a Mixing Time of 800 ms[a]

residue & atom		residue & atom[b]		NOE experiment	NOE prediction[c]
1	H5	1	H1	6.1 ± 0.6	8.9
1	H3	1	H1	4.1 ± 0.4	6.8
2	H3	2	H1	9.9 ± 1.0	5.6
2	H5	2	H1	13.2 ± 1.3	10.3
F1	H2	F1	H1	8.8 ± 0.9	9.9
F1	H3	F1	H5	7.9 ± 0.8	9.3
F1	H4	F1	H5	10.7 ± 1.1	11.0
F2	H2	F2	H1	13.3 ± 1.3	12.0
F2	H3	F2	H5	8.4 ± 0.8	9.3
F2	H4	F2	H5	14.5 ± 1.5	11.2
2	H3	1	H1	4.4 ± 0.4	8.9
3	H3	2	H1	16.5 ± 1.7	14.7
4	H4	3	H1	12.7 ± 1.3	14.9
1	H2	F1	H1	8.5 ± 0.9	9.7
2	H2	F1	H5	9.3 ± 0.9	10.0
2	H4	F1	H5	2.0 ± 0.2	1.5
2	H3	F2	H1	0.6 ± 0.1	0.4
2	H4	F2	H1	9.8 ± 1.0	8.5
2	H5	F2	H1	1.7 ± 0.2	1.4
1	H2	F2	H5	8.4 ± 0.8	10.3
2	H3	F2	H5	1.1 ± 0.1	0.9
2	H4	F2	H5	2.4 ± 0.2	1.9

[a] $\chi^2 = 246.5$, 22 points. F1 and F2 are the α(1 → 2) and α(1 → 4) linked fucose residues, respectively. Residues 1, 2, 3, and 4 are Gal β(1 → 3), GlcNAc, Gal β(1 → 4) and Glc, respectively. [b] NOESY cross-peaks were normalized against the diagonal peak corresponding to the atom described in the second set of columns. [c] Theoretical calculation, assuming no internal motion and isotropic tumbling, $\tau_c = 0.50$ns.

have been developed for calculating alignment tensors directly from molecular shape (*18*, *32*) based on steric obstruction of isotropic rotation, in addition to the standard techniques of back-calculating alignment tensors from experimental data, for example, using singular value decomposition (*28*). In such a theory of steric obstruction (*18*), the alignment tensor is hypothesized to be diagonal in the principal frame of the radius of gyration tensor, and hence possesses three (nonindependent) components. Figure 5 shows how the predicted diagonal components of the alignment tensor would vary throughout the simulation of each oligosaccharide (S_{11} corresponds to the principal axis, where alignment is greatest). It can be seen that fucosyllactose has a qualitatively different set of predictions than the other two oligosaccharides, because it has a different molecular symmetry. If *a*, *b*, and *c* are its principal lengths from largest to smallest, then $a \approx b$ and $c \ll a$, which describes a flattened disk. In contrast, both LNF-1 and LND-1 have shapes in which $b \approx c$ and $a \gg b$, which describes an elongated cylinder or rod. These two shapes, a disk and a rod, represent the two extremes of alignment by

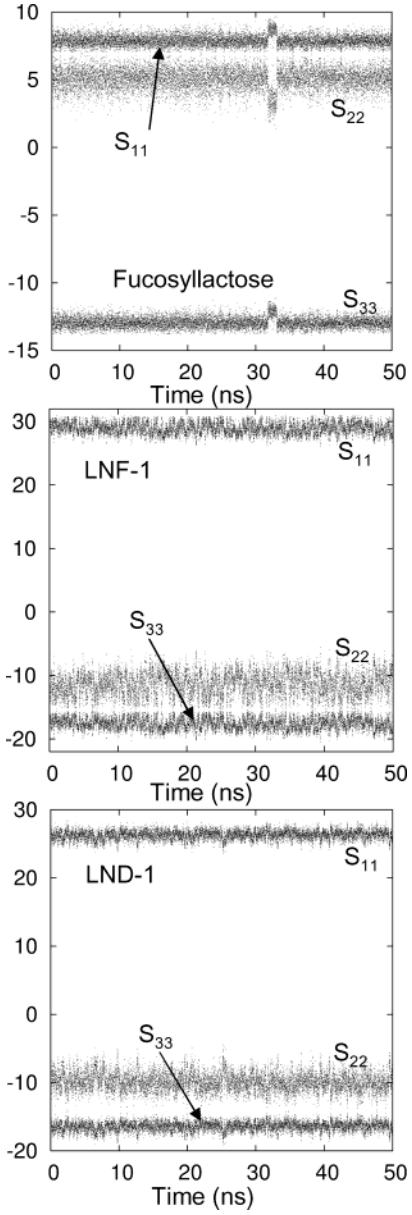

FIGURE 5: Predicted alignment tensors based on a theory of steric alignment by neutral media for the three oligosaccharides during each simulation. From top to bottom: fucosyllactose, LNF-1, and LND-1. The shape of fucosyllactose approximates to a disk, while LNF-1 and LND-1 approximate to an elongated cylinder.

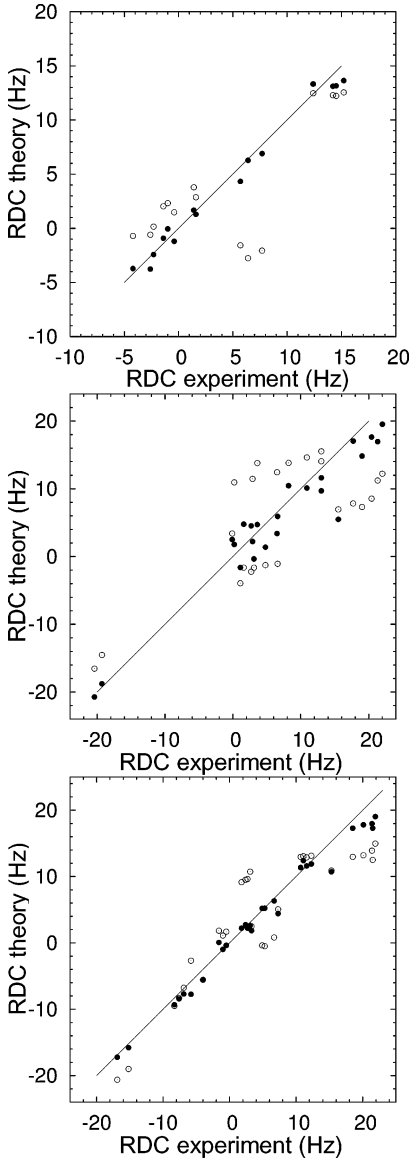

FIGURE 6: Comparison of experimental measurements against residual dipolar couplings (RDCs) predicted on the basis of a theory of steric alignment (open circles), and singular value decomposition (solid circles). From top to bottom: fucosyllactose, LNF-1, and LND-1.

molecular shape, and are therefore important examples. Extraction of the one-bond direction vectors and utilization of the alignment tensors calculated above allow the average dipolar coupling to be predicted from simulations. The theoretical predictions based on steric alignment, and their correlation with experimental data is shown in Figure 6 using open circles.

Improved Alignment Tensor Calculation. Although residual dipolar couplings calculated from simulations using steric alignment and experimental data are in trend agreement, the correlation is weaker than obtained previously (*16*, *17*). Since the simulations agreed with experimental NOESY data, it is possible that the disagreement is due to inadequacies in prediction of the alignment tensor, assuming that the oligosaccharides maintained their conformational equilibrium during alignment. The alignment tensor for the whole molecule was therefore recalculated at each stage of the simulation using the experimental data and the method of singular value decomposition, which effectively solves the least-squares problem to obtain the alignment tensor (*28*). Such a direct approach is only appropriate when a single conformation dominates, as in these simulations. Although not a prerequisite, the alignment tensor was found to be approximately diagonal in the principle frame of the radius of gyration tensor. For fucosyllactose, the calculated alignment tensors are not dissimilar to those shown in Figure 5; the magnitude of S_{11} decreases and S_{33} increases slightly. However, for LNF-1 and LND-1 the tensors calculated by the two methods are significantly different. In this case, the diagonal components are proportional to (1, 0, −1) rather than (1, −1/2, −1/2) calculated by the steric method. These calculated alignment tensors can again be used to make predictions of residual dipolar couplings for the three oligosaccharides; their correlation with experimental observations is shown in Figure 6 using solid circles. Therefore, although the simulation can, in principle, agree with the experimental data, it would appear that the alignment is not fully described by the steric methodology.

Microscopic Analysis of the Simulations. Figure 2 shows the hydrogen bonds predicted for the fucosyllactose oligosaccharide. Across the $\beta(1 \rightarrow 4)$ a hydrogen bond is predicted between OH3 and O5 (labeled C), as found in crystal structures of cellulose. The persistence of this hydrogen bond is very high as shown in Figure 7a, and consequently the $\beta(1 \rightarrow 4)$ linkage is observed to be highly restricted. However, interactions across the $\beta(1 \rightarrow 4)$ linkage involving the galactose hydroxymethyl are infrequent because this moiety interacts strongly with its own O4 hydroxyl for a large part of the simulation (labeled B). Across the $\alpha(1 \rightarrow 2)$ linkage a weak hydrogen bond can be formed between O2 and O3 (labeled A). Although O2 and O3 stay proximal throughout the simulation, interactions with water molecules are predicted to be favored at this linkage, and consequently the $\alpha(1 \rightarrow 2)$ linkage has a rather large conformational freedom, compared with the $\beta(1 \rightarrow 4)$ linkage.

The oligosaccharide LNF-1, which contains an epitope similar to fucosyllactose, possesses a similar set of interactions, Figure 3. Again, the hydroxymethyl group of Gal can interact with its own O4 moiety (C and E), and O2 and O3 interact across the $\alpha(1 \rightarrow 2)$ linkage through a set of dynamic water interactions (B), detailed in Figure 7b. In this case, steric hindrance is predicted to remove some of the conformational flexibility at the linkage, resulting from incorporation of a GlcNAc sugar rather than Glc (as in fucosyllactose). This *N*-acetyl group can interact with O2 of the Fuc residue (A), made possible by the fact that the linkage is now a $\beta(1 \rightarrow 3)$ linkage rather than the $\beta(1 \rightarrow 4)$ found at the same point in fucosyllactose. In this case, a hydrogen bond between OH4 and O5 is observed across the linkage (D), less persistent than the OH3···O5 hydrogen bond observed in fucosyllactose and the $\beta(1 \rightarrow 3)$ linkage is consequently more diffuse than the similar $\beta(1 \rightarrow 4)$ linkage. However, at the second $\beta(1 \rightarrow 3)$ linkage, the hydroxyl normally available for a hydrogen-bonding interaction with O5, OH4, is epimerized in Gal. This results in a change in the hydrogen-bonding dynamics, causing the hydroxymethyl group and OH4 to interact within the Gal residue itself (E), and the $\beta(1 \rightarrow 3)$ linkage to be bridged by many water molecules; consequently this linkage becomes more flexible than expected. On the other hand, the behavior of the terminal $\beta(1 \rightarrow 4)$ linkage is as expected for this type of linkage,

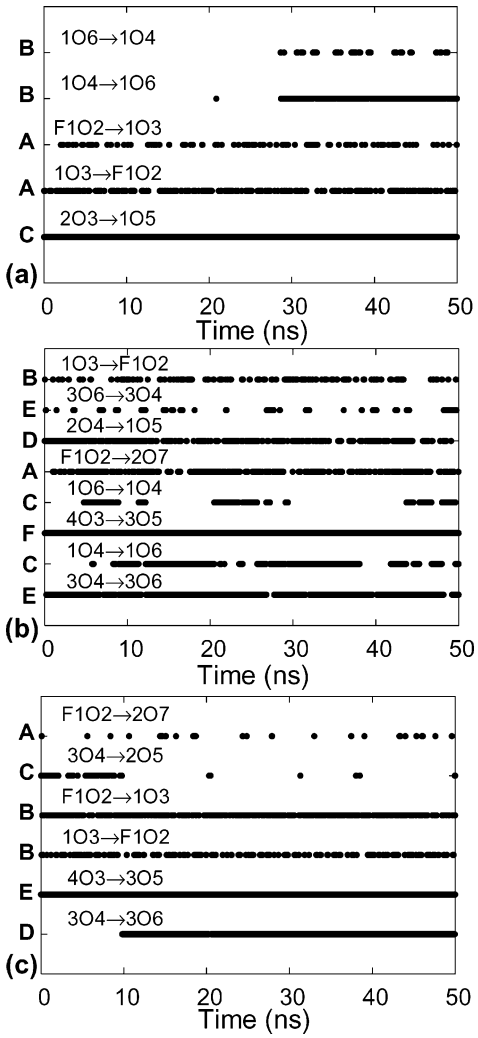

FIGURE 7: The most persistent intramolecular hydrogen bonds observed in (a) fucosyllactose; see Figure 2 for the key to the letters on the left-hand side, (b) LNF-1; see Figure 3 for the key, and (c) LND-1; see Figure 4 for the key.

with previously observed water interactions, resulting in a strong interaction between O3 and O5 (F).

The chemical structure of LND-1 is similar to LNF-1, with the addition of an extra fucose. Dynamic interactions at the linkages of LND-1 are therefore expected to be similar to LNF-1, and this was observed in the simulations, Figure 4. However, the steric hindrance imposed by the additional fucose residue resulted in restrictions at both the $\alpha(1 \rightarrow 2)$ linkage and the adjacent $\beta(1 \rightarrow 3)$ linkage results in restriction at the $\beta(1 \rightarrow 3)$ linkage, as compared with LNF-1, and the $\alpha(1 \rightarrow 2)$ linkage becomes slightly more restricted. Water interactions at the reducing end of the molecule are identical to those in LNF-1; compare Figure 7, panels b and c. The interaction O4···O5 at the $\beta(1 \rightarrow 3)$ linkage (C), however, persists for some 10 ns before it adopts the O6···O4 hydrogen bond (D), as found in LNF-1, for the remainder of the simulation. This suggests that the O4···O5 hydrogen bond is merely an effect of the starting configuration of the simulation.

Statistical information on the conformation of the hydroxymethyl groups could not be obtained because only a maximum of two transitions per sugar residue was observed. This is a significantly lower frequency than observed in monosaccharides, for example, where over 10 transitions were typically observed in a 50 ns period in aqueous solution (*33*). This indicated that conformational transitions in the hydroxymethyl groups of oligsosaccharides are less frequent than in monosaccharides, by an order of magnitude.

DISCUSSION

Simulations and NOESY analysis confirmed that a single $\alpha(1 \rightarrow 2)$ linkage conformation is most likely for fucosyllactose, as described previously (*34*, *35*). In this conformation, the molecule has a flattened disk shape, which places Fuc H5 and Glc H5 in close proximity, with a relatively well-defined structure. Langevin simulations, performed previously in vacuo, came to a similar conclusion, and were able to predict scalar couplings ($^3J_{CH}$) in reasonable agreement with an experiment (*30*) using an empirical equation (*36*). Recalculation of these scalar couplings using the present simulations results in the following values (experimental values in parentheses): 2.9 Hz (3.6 Hz), 4.4 Hz (5.3 Hz), 2.5 Hz (3.5 Hz) for $^3J_{HCOH}$ and $^3J_{COCH}$ at the $\alpha(1 \rightarrow 2)$ linkage and $^3J_{HCOC}$ at the $\beta(1 \rightarrow 4)$ linkage, respectively. The values predicted from these simulations are in closer agreement than those published previously (*30*), perhaps due to the presence of water. Further agreement may not be possible until more accurate Karplus equations become available (*17*, *37*).

Molecular dynamics simulations suggested that the terminal regions of LNF-1 could adopt a similar conformation to fucosyllactose, albeit with a slightly more restricted $\alpha(1 \rightarrow 2)$ linkage. This model was consistent with NOESY data, and restricted molecular motion (*38*). Although conformational exchange has been predicted at the $\beta(1 \rightarrow 4)$ linkage of lactose (*39*), no such conformational equilibrium was observed in these aqueous simulations. A single conformational population was realized, which agrees with other molecular mechanics calculations, experimental data, and crystal structures of lactose in complex with ricin B-chain, for example (*15*, *40*). It is also in agreement with recent molecular modeling studies of $\beta(1 \rightarrow 4)$ linkages which indicate that water molecules can stabilize a rigid conformation at this linkage (*41*).

The hexasaccharide LND-1 differs from LNF-1 by a single $\alpha(1 \rightarrow 4)$ linked fucose, a change that converts the terminal blood-group H-antigen of LNF-1 into a Lewis-B epitope. Such an addition is predicted to leave the core structure unchanged, and add a little extra steric restriction to the $\alpha(1 \rightarrow 2)$ linkage, as compared with LNF-1. Results from NOESY confirmed this, evidence for the conformation predicted by molecular dynamics simulations. Grid searches and Monte Carlo methods using the MM3 force-field in vacuo (*11*) have previously identified a single conformational minima for the $\alpha(1 \rightarrow 4)$ linkage in agreement with the simulations presented here. Detailed analysis of the Lewis-B epitope indicated that the Fuc residues have an average conformation close to that predicted by the molecular dynamics simulations performed here (*42*).

Measurements conducted at 800 MHz proton frequency allowed enhanced chemical shift dispersion and hence a larger dipolar coupling data set to be collected than previously possible for LNF-1 and LND-1 (*10*). This is particularly important because CH vectors in carbohydrate (chair) rings have only two linearly independent directions (equato-

rial and axial). Such linear dependency is particularly problematic if one wishes to back-calculate the alignment tensor of individual sugar rings (*43*), and in this case extra information is necessary, such as homonuclear residual dipolar couplings. However, with the aid of the MD simulation vectors can be considered with respect to the molecule as a whole. Thus, there are up to 10 linearly independent vectors (in LND-1) with respect to the molecular frame. Therefore, changes in molecular conformation anywhere in the molecule lead to changes in the molecular alignment tensor, and thus the $^1J_{CH}$ dipolar coupling set are sensitive to overall conformation.

For LNF-1, no simple scaling relation was found between residual dipolar couplings induced by phages and previous measurements made in the presence of bicelles (*10*). Alignment therefore may be described by two different tensors in the two cases, suggesting that the idea of steric alignment (*18*), which would require identical tensors, is not appropriate for this oligosaccharide in either phage, bicelle or both. Conversely, residual dipolar couplings measured for LND-1 in both phage and bicelle (*10*) were found to have a closer linear relationship, and are both in reasonable agreement with the aqueous molecular dynamics predictions for LND-1 presented. Therefore, it is possible that for highly anisotropic molecules such as LNF-1, which is a rod with a protruding side sugar, the steric alignment model breaks down. However, in LND-1, which has a second fucose, the anisotropic effects of the first are proposed to be balanced out to some extent by the second. Such a hypothesis is supported by alignment tensors calculated by singular value decomposition (Figure 6), which indicates that both LNF-1 and LND-1 have large anisotropies. In such a case, the alignment is exquisitely sensitive to conformational parameters. The observed discrepancies may also be due, in part, to that the aligning cosolute altering the conformational equilibrium of the oligosaccharides (*44*), a conclusion that cannot be ruled out by these studies.

In an oligosaccharide with an $\alpha(1 \rightarrow 6)$ linkage, the fit to the experimental residual dipolar coupling data could be improved by mixing multiple conformations (*17*). However, in this case there is no evidence for conformations other than the ones presented here which could improve the fit to the residual dipolar coupling data. Similarly, NOEs across glycosidic bonds did not support the idea that other major conformational states exist, supporting the hypothesis that these molecules form relatively ordered structures in solution. Previous conformational studies of blood-group oligosaccharides have yielded mixed conclusions. Some studies have proposed that the molecules have unique conformations (*45*), while others have indicated the presence of conformational mixtures (*46*). The simulations here show that interactions with water molecules in these oligosaccharides result in dynamic molecules that are essentially librations about an average conformation. This has been described as "motion of the first kind" (*47*), where rapid motion of the linkage occurs on the picosecond time scale, effectively Gaussian motion closely centered on a single local minimum. Such structures can be approximated by static structures relatively straightforwardly. Therefore, the alignment tensor and NOEs could, in this case, be approximated by an effective alignment tensor and an effective structure, to a reasonable approximation.

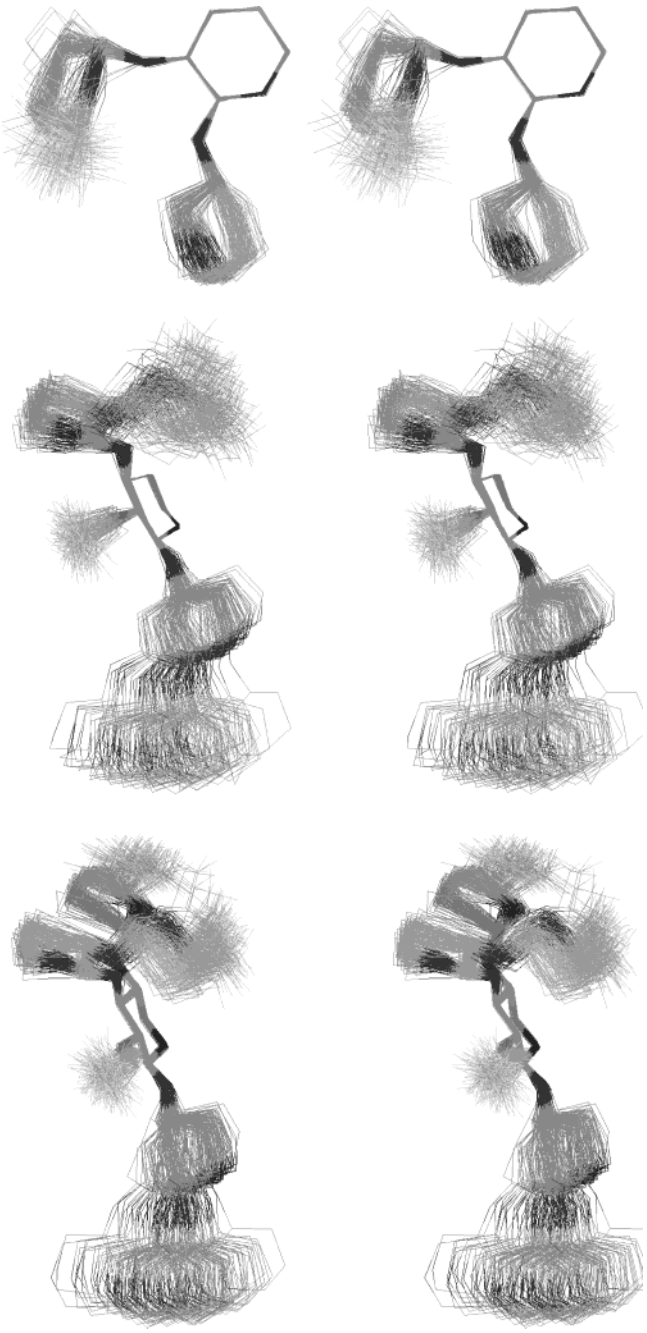

FIGURE 8: Predicted dynamic shapes of fucosylated oligosaccharides from aqueous molecular dynamics simulations visualized by minimizing the mean-square distance of a central sugar residue between frames and overlaying. Many side-groups have been removed for clarity. The stereo images are of (top) fucosyllactose, centered on Gal, (middle) LNF-1 centered on GlcNAc, and (bottom) LND-1, also centered on GlcNAc.

Since water is observed to restrict the flexibility of fucose sugars, the present limited availability of molecular dynamics simulations which contain explicit solvent (*38*, *48*) has perhaps led to predictions of blood-group oligosaccharides that are too flexible, and it is the dynamic shape of these molecules that leads to their biological activity. Following testing against experimental data, it is possible to visualize how the different oligosaccharides may exist in solution. This is depicted in Figure 8, where the Gal residue of fucosyllactose and the GlcNAc residues of LNF-1 and LND-1 have been overlaid by minimizing the mean square distance

between frames. It is evident that these fucoylated oligosaccharides have reasonably well-defined conformations, which is perhaps not surprising since they are key recognition molecules.

This study has shown how molecular dynamics, combined with experimental verification, can be used as a method for understanding both the interactions with water, and the structure and dynamics of complex oligosaccharides. This provides hope that soon such an approach will move structural biology from the static structures represented by X-ray crystallography to a new dynamic perspective. Such a perspective allows function to be appreciated and will inform the understanding of ligand−receptor interactions, which is essential for the design of carbohydrate-based pharmaceuticals.

ACKNOWLEDGMENT

We thank the Danish Instrument Centre for NMR Spectroscopy of Biological Macromolecules for providing time on their 800 MHz Varian Unity Inova NMR spectrometer.

SUPPORTING INFORMATION AVAILABLE

Tables of assignments and calculated one-bond residual dipolar couplings for the fucosyllactose, LNF-1, LND-1 oligosaccharides. This material is available free of charge via the Internet at http://pubs.acs.org.

REFERENCES

1. Campbell, I. D. (2002) The march of structural biology. *Nat. Rev. Mol. Cell Biol. 3*, 377−381.
2. Kempf, J. G., and Loria, J. P. (2003) Protein dynamics from solution NMR − theory and applications. *Cell Biochem. Biophys. 37*, 187−211.
3. Karplus, M., and McCammon, J. A. (2002) Molecular dynamics simulations of biomolecules. *Nat. Struct. Biol. 9*, 646−652.
4. Stevensson, B., Landersjo, C., Widmalm, G., and Maliniak, A. (2002) Conformational distribution function of a disaccharide in a liquid crystalline phase determined using NMR spectroscopy. *J. Am. Chem. Soc. 124*, 5946−5947.
5. Guillot, B. (2002) A reappraisal of what we have learnt during three decades of computer simulations on water. *J. Mol. Liq. 101*, 219−260.
6. Staudacher, E., Altmann, F., Wilson, I. B. H., and Marz, L. (1999) Fucose in N-glycans: from plant to man. *Biochim. Biophys. Acta 1473*, 216−236.
7. Bush, C. A., Yan, Z. Y., and Rao, B. N. N. (1986) Conformational energy calculations and proton nuclear Overhauser enhancements reveal a unique conformation for blood group-A oligosaccharides. *J. Am. Chem. Soc. 108*, 6168−6173.
8. Cagas, P., and Bush, C. A. (1990) Determination of the conformation of Lewis blood-group oligosaccharides by simulation of 2-dimensional nuclear Overhauser data. *Biopolymers 30*, 1123−1138.
9. Azurmendi, H. F., Martin-Pastor, M., and Bush, C. A. (2002) Conformational studies of Lewis X and Lewis A trisaccharides using NMR residual dipolar couplings. *Biopolymers 63*, 89−98.
10. Martin-Pastor, M., and Bush, C. A. (2000) Conformational studies of human milk oligosaccharides using ^{1}H-^{13}C one-bond NMR residual dipolar couplings. *Biochemistry 39*, 4674−4683.
11. Weimar, T., Peters, T., Perez, S., and Imberty, A. (1997) Combined NMR, grid search MM3 and Metropolis Monte Carlo GEGOP studies of two L-fucose containing disaccharides: α-L-Fuc-(1,4)-β-D-GlcNAc-OMe and α-L-Fuc-(1,6)-β-D-GlcNAc-OMe. *Theochem-J. Mol. Struct. 395*, 297−311.
12. Bush, C. A., and Yan, Z. Y. (1988) Molecular-dynamics simulations of blood group-A and group-H oligosaccharides. *Biophys. J. 53*, A101−A101.
13. Mukhopadhyay, C., and Bush, C. A. (1991) Molecular-dynamics simulation of Lewis blood-groups and related oligosaccharides. *Biopolymers 31*, 1737−1746.
14. Yan, Z. Y., and Bush, C. A. (1990) Molecular-dynamics simulations and the conformational mobility of blood-group oligosaccharides. *Biopolymers 29*, 799−811.
15. Rutenber, E., and Robertus, J. D. (1991) Structure of ricin B-chain at 2.5 Å resolution. *Proteins 10*, 260−269.
16. Almond, A., Bunkenborg, J., Franch, T., Gotfredsen, C. H., and Duus, J. Ø. (2001) Comparison of aqueous molecular dynamics with NMR relaxation and residual dipolar couplings favors internal motion in a mannose oligosaccharide. *J. Am. Chem. Soc. 123*, 4792−4802.
17. Almond, A., and Duus, J. Ø. (2001) Quantitative conformational analysis of the core region of N-glycans using residual dipolar couplings, aqueous molecular dynamics, and steric alignment. *J. Biomol. NMR 20*, 351−363.
18. Almond, A., and Axelsen, J. B. (2002) Physical interpretation of residual dipolar couplings in neutral aligned media. *J. Am. Chem. Soc. 124*, 9986−9987.
19. Meissner, A., Duus, J. Ø., and Sørensen, O. W. (1997) Integration of spin-state-selective excitation into 2D NMR correlation experiments with heteronuclear ZQ/2Q π-rotations for $^{1}J_{XH}$-resolved E.COSY-type measurement of heteronuclear coupling constants in proteins. *J. Biomol. NMR 10*, 89−94.
20. Pham, T. N., Liptaj, T., Bromek, K., and Uhrin, D. (2002) Measurement of small one-bond proton-carbon residual dipolar coupling constants in partially oriented (13)C natural abundance oligosaccharide samples: analysis of heteronuclear (1)J(CH)-modulated spectra with the BIRD inversion pulse. *J. Magn. Reson. 157*, 200−209.
21. Woods, R. J., Dwek, R. A., Edge, C. J., and Fraserreid, B. (1995) Molecular mechanical and molecular dynamical simulations of glycoproteins and oligosaccharides. 1. Glycam-93 parameter development. *J. Phys. Chem. 99*, 3832−3846.
22. Brooks, B. R., Bruccoleri, R. E., Olafson, B. D., States, D. J., Swaminathan, S., and Karplus, M. (1983) CHARMM − a program for macromolecular energy, minimization, and dynamics calculations. *J. Comput. Chem. 4*, 187−217.
23. Jorgensen, W. L., Chandrasekhar, J., Madura, J. D., Impey, R. W., and Klein, M. L. (1983) Comparison of simple potential functions for simulating liquid water. *J. Chem. Phys. 79*, 926−935.
24. Hockney, R. W. (1970) The potential calculation and some applications. *Methods Comput. Phys. 9*, 135−211.
25. Verlet, L. (1967) Computer experiments on classical fluids. I. Thermodynamical properties of Lennard-Jones molecules. *Phys. Rev. 159*, 98−103.
26. van Gunsteren, W. F., and Berendsen, H. J. C. (1977) Algorithms for macromolecular dynamics and constraint dynamics. *Mol. Phys. 34*, 1311−1327.
27. Brady, J. W., and Schmidt, R. K. (1993) The role of hydrogen-bonding in carbohydrates: molecular-dynamics simulations of maltose in aqueous solution. *J. Phys. Chem. 97*, 958−966.
28. Losonczi, J. A., Andrec, M., Fischer, M. W. F., and Prestegard, J. H. (1999) Order matrix analysis of residual dipolar couplings using singular value decomposition. *J. Magn. Reson. 138*, 334−342.
29. Lipari, G., and Szabo, A. (1982) Model-free approach to the interpretation of nuclear magnetic-resonance relaxation in macromolecules. 1. Theory and range of validity. *J. Am. Chem. Soc. 104*, 4546−4559.
30. Rundlof, T., and Widmalm, G. (2001) NMR analysis of the trisaccharide 2′-fucosyllactose by heteronuclear trans-glycosidic coupling constants and molecular simulations. *Magn. Reson. Chem. 39*, 381−385.
31. Krishnan, V. V., and Cosman, M. (1998) An empirical relationship between rotational correlation time and solvent accessible surface area. *J. Biomol. NMR 12*, 177−182.
32. Azurmendi, H. F., and Bush, C. A. (2002) Tracking alignment from the moment of inertia tensor (TRAMITE) of biomolecules in neutral dilute liquid crystal solutions. *J. Am. Chem. Soc. 124*, 2426−2427.
33. Kirschner, K. N., and Woods, R. J. (2001) Solvent interactions determine carbohydrate conformation. *Proc. Natl. Acad. Sci. U.S.A. 98*, 10541−10545.
34. Ishizuka, Y., Nemoto, T., Fujiwara, M., Fujita, K., and Nakanishi, H. (1999) Three-dimensional structure of fucosyllactoses in an aqueous solution. *J. Carbohydr. Chem. 18*, 523−533.
35. Widmalm, G., and Venable, R. M. (1994) Molecular-dynamics simulation and NMR-study of a blood group-H trisaccharide. *Biopolymers 34*, 1079−1088.

36. Tvaroska, I., Hricovini, M., and Petrakova, E. (1989) An attempt to derive a new Karplus-type equation of vicinal proton-carbon coupling-constants for C−O−C−H segments of bonded atoms. *Carbohydr. Res. 189*, 359−362.
37. Brüschweiler, R., and Case, D. A. (1994) Adding harmonic motion to the Karplus relation for spin−spin coupling. *J. Am. Chem. Soc. 116*, 11199−11200.
38. Rundlof, T., Venable, R. M., Pastor, R. W., Kowalewski, J., and Widmalm, G. (1999) Distinguishing anisotropy and flexibility of the pentasaccharide LNF-1 in solution by carbon-13 NMR relaxation and hydrodynamic modeling. *J. Am. Chem. Soc. 121*, 11847−11854.
39. Espinosa, J. F., Canada, F. J., Asensio, J. L., Martin-Pastor, M., Dietrich, H., Martin-Lomas, M., Schmidt, R. R., and Jimenez-Barbero, J. (1996) Experimental evidence of conformational differences between C-glycosides and O-glycosides in solution and in the protein-bound state: The C-lactose/O-lactose case. *J. Am. Chem. Soc. 118*, 10862−10871.
40. Oh, J., Kim, Y., and Won, Y. (1995) Conformational analysis and molecular dynamics simulation of lactose. *Bull. Korean Chem. Soc. 16*, 1153−1162.
41. Almond, A., and Sheehan, J. K. (2003) Predicting the molecular shape of polysaccharides from dynamic interactions with water. *Glycobiology 13*, 255−264.
42. Bekiroglu, S., Sandstrom, C., Norberg, T., and Kenne, L. (2000) Hydroxy protons in conformational study of a Lewis B tetrasaccharide derivative in aqueous solution by NMR spectroscopy. *Carbohydr. Res. 328*, 409−418.
43. Neubauer, H., Meiler, J., Peti, W., and Griesinger, C. (2001) NMR structure determination of saccharose and raffinose by means of homo- and heteronuclear dipolar couplings. *Helv. Chim. Acta 84*, 243−258.
44. Berthault, P., Jeannerat, D., Camerel, F., Alvarez Salgado, F., Boulard, Y., Gabriel, J. C., and Desvaux, H. (2003) Dilute liquid crystals used to enhance residual dipolar couplings may alter conformational equilibrium in oligosaccharides. *Carbohydr. Res. 338*, 1771−1785.
45. Azurmendi, H. F., and Bush, C. A. (2002) Conformational studies of blood group A and blood group B oligosaccharides using NMR residual dipolar couplings. *Carbohydr. Res. 337*, 905−915.
46. Imberty, A., Mikros, E., Koca, J., Mollicone, R., Oriol, R., and Perez, S. (1995) Computer-simulation of histo-blood group oligosaccharides − energy maps of all constituting disaccharides and potential-energy surfaces of 14 ABH and Lewis carbohydrate antigens. *Glycoconjugate J. 12*, 331−349.
47. Martin-Pastor, M., and Bush, C. A. (1999) New strategy for the conformational analysis of carbohydrates based on NOE and ^{13}C NMR coupling constants. Application to the flexible polysaccharide of Streptococcus mitis J22. *Biochemistry 38*, 8045−8055.
48. Corzana, F., Bettler, E., du Penhout, C. H., Tyrtysh, T. V., Bovin, N. V., and Imberty, A. (2002) Solution structure of two xenoantigens: α-Gal-LacNAc and α-Gal-Lewis X. *Glycobiology 12*, 241−250.

BI0354886